We are IntechOpen, the world's leading publisher of Open Access books Built by scientists, for scientists

4,800
Open access books available

122,000
International authors and editors

135M
Downloads

Our authors are among the

154
Countries delivered to

TOP 1%
most cited scientists

12.2%
Contributors from top 500 universities

CLARIVATE ANALYTICS BOOK CITATION INDEX INDEXED

WEB OF SCIENCE™

Selection of our books indexed in the Book Citation Index in Web of Science™ Core Collection (BKCI)

Interested in publishing with us?
Contact book.department@intechopen.com

Numbers displayed above are based on latest data collected.
For more information visit www.intechopen.com

8

Polarimetric responses and scattering mechanisms of tropical forests in the Brazilian Amazon

J. R. dos Santos[1], I. S. Narvaes[1], P. M. L. A. Graça[2] and F. G. Gonçalves[3]
(1) INPE - National Institute for Space Research
Av. dos Astronautas, 1758 CEP.:12.227-010 São José dos Campos – SP., Brazil
Email: {jroberto, igor}@dsr.inpe.br
(2) INPA - National Institute of Amazonian Research
Av. André Araujo, 2936 CEP.: 69060-001 Manaus – AM., Brazil,
Email: pmlag@inpa.gov.br
(3) Oregon State University
Department of Forest Ecosystems and Society, Corvallis, OR 97331 EUA,
Email: fabio.goncalves@oregonstate.edu

Abstract
This chapter discusses the polarimetric responses of PALSAR (L-band) data and scattering mechanisms of some tropical forest typologies based on target decomposition. The fundamentals of polarimetric theory related to both SAR topics under development are summarized. For representation of polarimetric signatures, the cross-section of the forest target (σ) was plotted on a bi-dimensional graphic as a function of the orientation angle, ellipticity angle and the intensity of co-polar components of the radar signal. The analysis of scattering mechanisms was done by the association of entropy and mean alpha angle values of each sample, plotted in a bi-dimensional classification space. This study improves the understanding of the interaction mechanisms between L-band PALSAR signals and structural parameters, supporting the forest inventory in the Brazilian Amazon region.
KEYWORDS: tropical forest, polarimetric signatures, target decomposition, PALSAR, monitoring.

1. Introduction

The ongoing particular and governmental struggle over the Brazilian Amazon's future mirror broader current discourses on the "environment" (Andersen et al., 2002), experts and layperson alike vary widely along continuum perspectives, based on two scenarios: (a) the line of defenders of global ecological services ("conservationists") and (2) the focus of development interests in the countries hosting these forests ("developmentalists"). They both present an important view points and significant arguments. While these discussions

occur in the frame of a possible territorial planning, the degradation process with habitat fragmentation is still going on, with an estimative of rate gross deforestation in the Amazon region of around 11,968 km² (timeframe of 2007-2008), with an error of approximately 4% (<http://www.obt.inpe.br/prodes/index.html>). Due to the advancement of economic activities in the domain of the Brazilian Amazon tropical rainforest, remote sensing have being used as a fundamental tool to characterize the causes of degradation (conversion of natural vegetation to agriculture and cattle raising, selective logging, charcoal production, etc.), and also to monitor the impact of human activities over these large ecosystems.

Taking into account that in tropical regions there is, all over the year, a high percentage of cloud cover which impedes the inventory and updating of the forest cover by optical data, it is important to use sensor systems which operate at microwave wavelengths. A multi-temporal analysis of TM-Landsat data (timeframe of 12 years) used to estimate the annual gross deforestation rate in the Brazilian Amazon region showed that in average 21.12% of the imaged areas was cloud covered (Santos et al., 2008). Since there is a significant dynamic in environments of the Amazon region due to seasonal variations or from the different conditions resulting from human action, it is important to use radar images to understand the transformation process in the forest landscape.

To briefly introduce a reader on this subject, including concepts and applications of radar data in forestry studies, the following papers are recommended: Ulaby and Elachi (1990), Beaudoin et al. (1994), Henderson and Lewis (1998) and Coops (2002). These authors studied multitemporal SAR (Synthetic Aperture Radar) backscatter for discriminating forest types, discussing those conditions of scattering and attenuation of radar signals at different frequencies interacting with structural vegetation features. Pope et al. (1994) developed indices based on ratios and normalized different of multipolarimetric radar data, which can be related to certain characteristics of vegetation cover, such as e.g. biomass, canopy structure, volume scattering, applied to tropical forest in Central America. Hoekmann and Quiñones (2000), Hawkins et al. (2000) and Santos et al. (2002; 2003) correlated information obtained from radar with forest biomass levels, discussing the saturation of backscatter saturation caused by the high density of tropical forests. Power spectrum analysis was made using autoregressive moving-average (ARMA) models, for evaluation of forest canopy structure from airborne SAR (X–band) data in the Brazilian Amazon (Neeff et al., 2005a). This approach is novel where the radar spectra match those obtained from ground data, establishing the basis for the use of this relationship in spatial structure analysis of ecosystems from remote sensing sources. In more recent studies, and exploring the radar potentialities beyond its traditional polarimetric characteristics, Kugler et al. (2006) and Treuhaft et al. (2006) used interferometric radar data to estimate biophysical parameters in tropical forest areas. Using another approach, Neeff et al. (2005b) explored, through the local maximum filter technique (Wulder et al., 2000) and statistical Markov processes (Cressie, 1993) the interferometric height derived from airborne SAR (X- and P- bands) for the analysis of spatial forest patterns (three dimensional canopy structure and distances of very large trees). The above mentioned studies exemplify the importance of radar information in the analysis of tropical environments.

Within this frame, the objective of this chapter is to explorer the polarimetric mode, by the analysis of the graphic representation of signatures from PALSAR/ALOS data (L-band) in primary forest, secondary succession (initial, intermediate and advanced levels of natural recovery) and also, forests with timber exploitation. Additionally, we also discuss an

exploratory analysis of scattering mechanisms of tropical forest typology, in accordance with the alternative procedure of SAR image classification based on target decomposition.

1.1 Theoretical background

In order to understand the theme of this chapter, it is necessary to introduce some concepts about SAR polarimetry and of the classification technique based on target decomposition, as described below.

1.1.1 Concepts of polarized waves

Through different polarizations of radar imaging, the polarimetric signature of a certain target can be obtained, as well as the characterization of the dominant mechanism which controls the interaction of the microwave signal with the structure of the target under consideration.

The principle of polarimetry is related to the state of polarization of the wave, represented by definition as the electric field from the transmitting and receiving antenna. The state of polarization is described as an arbitrary set of axis used to describe horizontal polarized waves in the *x* axis (H polarization) and at the vertical polarized waves in the *y* axis (V polarization) along the wave propagation plan (*z),* which corresponds to the pointing direction of the antenna to the target. In this way, four types of polarization are obtained: HH for transmission and reception at the horizontal plan; VV for transmission and reception at the vertical plan; HV for transmission at the horizontal plan and reception at the vertical plan; and finally, VH for vertical transmission and horizontal reception. Ulaby and Elachi (1990) and Henderson and Lewis (1998) discuss how the electric field of an irradiated electromagnetic wave could be mathematically represented by a polarization ellipse. The polarization ellipse (Figure 1) is described by the three geometric parameters: the orientation angle ($-90^o < \psi < +90^o$), the ellipticity angle ($+45^o > \chi > -45^o$) and amplitude (A). The flattening factor from the ellipsis is given by angle χ, and there is a linear polarization when $\chi = 0$; the circular polarization to the left and right when $\chi = -45^o$ and $\chi = +45^o$, respectively. At the condition of $\chi = 0^o$ and $\psi = 0^o$ there is horizontal polarization and at $\chi = 0^o$ and $\psi \pm 90^o$ a vertical polarization. The analyst, who will discuss the polarization ellipse based on some literature references, must pay attention at the representation scale from the orientation axis, because graphical plots are presented in two forms: one of them with the polarization power varying between 0^o and 180^o, and the other varying from -90^o to $+90^o$, which can cause an interpretation error.

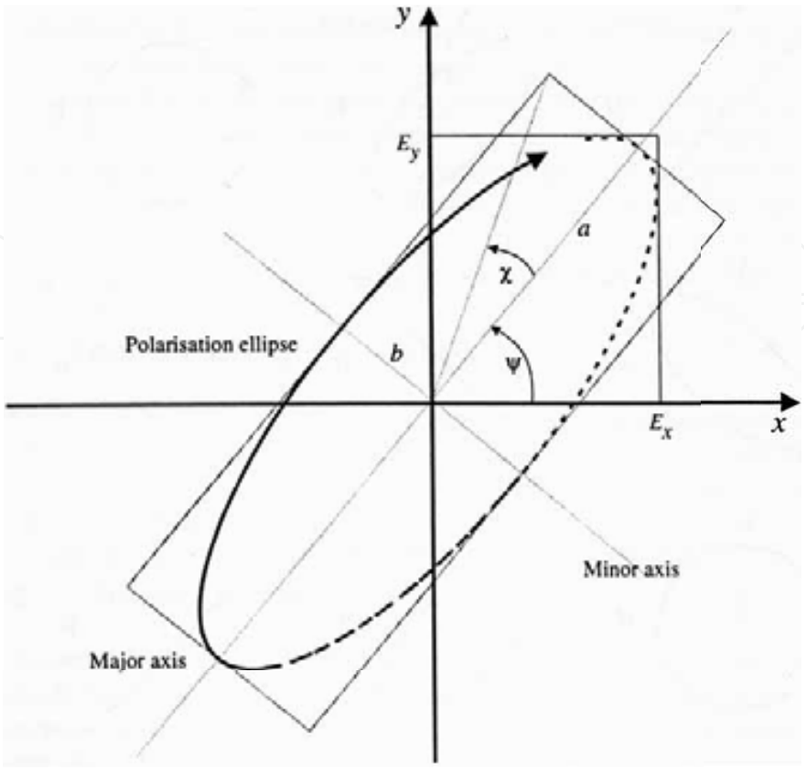

Fig. 1. Polarization pattern in the x-y plane, rotation angle ψ, ellipticity angle χ and auxiliary angle α. The size of the ellipse is governed by the maxima of the horizontal and vertical electrical field components. Source: Woodhouse (2006).

It is important to comment that the description of the wave polarization can be different according to the convention being considered. In the Forward Scattering Alignment (FSA) system, the wave propagation axis changes its direction after interaction with the target (this case represents the waves scattered by forest targets). In the Back Scattering Alignment (BSA) system the x and y axis are aligned in the same direction, and the wave propagation axis (z) is considered parallel, with the advantage of some mathematical simplifications on how the data are described (Woodhouse, 2006). In this way the coordinate system does not influence the nature of polarization, but just the way how the data are described.
There are other ways to represent the polarization state: (1) the graphic representation with the Poincaré sphere (Ulaby and Elachi, 1990), where the circular polarizations to the right and left are represented at the north and south poles respectively, while the intermediate polarization states are located at the regions between these poles. In this representation the meridians correspond to different inclination angles of the largest axis of the ellipse ($\psi = 0$) and the parallels to the ellipticity of the electric field ($\chi = \arctan(-B/A)$); (2) the mathematical representation by Jones vector, where the complex data received from each pulse emitted after the wave interacted with a target is demodulated at in-phase (In) and quadrature (Q) and converted to the digital format. Therefore, this mathematic representation is important because there is a direct relation with the polarization ellipse (van der Sanden, 1997; Woodhouse, 2006); (3) the Stokes vector where the polarized waves

can be characterized by four real and measurable parameters, with the same physical dimension, but only three are independent and describe the polarization state as:

$$I_0^2 = Q^2 + U^2 + V^2 \quad (1)$$

Where: Q = is the tendency of more vertical (Q > 0) or horizontal polarization (Q < 0);
U = expresses the tendency to be polarized at +45º (U > 0) and - 45º (U < 0);
V = polarization referring to the rule of right (V < 0) and left (V > 0) hand rules.

The parameters U and V are sometimes referred as being co-variances in-phase (real) and quadrature (imaginary), respectively between the components of the vertical and horizontal field of the wave. This expression is applied to completely polarized waves (amplitude and phase are invariant in time). Additionally the Stokes vector has a direct relation with the Poincaré sphere, because its ray is the Stokes parameter I_o (Woodhouse, 2006).

It is important to mention that the first imaging radars known as "conventional" recorded only information about the amplitude of the electric field at components *x* and *y*, i.e. the maximum magnitude of the electric field from a wave as a measurable indicator of size (van der Sanden, 1997). The amplitude takes into account the texture and brightness of the image, influenced by the surface roughness (macro-, meso- and micro-scales) and by the dielectric constant (moisture content of the target). With the advancement of technology, imaging radars started to record, phase information (the angular position δ of an oscillating movement at a defined instant in time *t*, as a function of the distance radar to target) in addition to amplitude, being called polarimetric radars. Such phase information provides information about the scattering mechanisms occurring in the imaged scene.

To improve the knowledge of the microwave interaction process with a certain target, it is necessary to understand the types of scatterers involved. The deterministic scatterers, also called coherent or punctual targets, are those where the interaction with electromagnetic waves reflects completely polarized waves, preserving the polarization of the incident wave (ESA, 2009a). Examples of this are urban targets. The non-deterministic targets, also known as incoherent targets or partially polarized or random distributed scatterers, are those that have more than one center of scattering, where the measured signal is the overlapping of a large amount of waves with variable polarization (ESA, 2009a). This is the case of forest targets. The change of polarization state is known as depolarization, caused mainly by multiple scattering due to surface roughness and to volumetric interaction with the target. Besides that, there is an almost specular reflection for smooth undulating surfaces, whose physical concept and representations will be presented below, when we consider the target decomposition approach.

1.1.2 Targets decomposition

In the polarimetric imaging the four complex components derived from the backscattering in each resolution cell (S_{HH}, S_{HV}, S_{VH}, S_{VV}) can be expressed by a scattering matrix [S] which, according to Ulaby and Elachi (1990) is given by:

$$[S] = \begin{pmatrix} S_{VV} & S_{VH} \\ S_{HV} & S_{HH} \end{pmatrix} \quad (2)$$

According to Woodhouse (2006), the scattering matrix [S] is applied to deterministic targets (coherent), and models how the scatterers transform the components of the incident electric field (E^i) in the scattered electric field (E^s).

$$\begin{pmatrix} E_v^s \\ E_h^s \end{pmatrix} = \frac{e^{-ik_0 r}}{R} \begin{pmatrix} S_{VV} & S_{VH} \\ S_{HV} & S_{HH} \end{pmatrix} \begin{pmatrix} E_v^i \\ E_h^i \end{pmatrix} \tag{3}$$

Where R is the distance from the antenna to the target and $k = 2\pi / \lambda$

Non-deterministic targets (incoherent) are represented by second order matrices. When the polarization of the electromagnetic wave is represented by the modified Stokes vector, the relation between the polarization of the incident electric field F^i and the scattered field F^s is given by the Müller matrix [M] (or Stokes matrix) in the FSA system, or also by the Kennaugh matrix [K] in the BSA system (Woodhouse, 2006), according to the equations below:

$$\left\langle F^s \right\rangle = \frac{1}{r^2}[M]\left\langle F^i \right\rangle \tag{4}$$

$$\left\langle \overline{F}^s \right\rangle = \frac{1}{r^2}[K]\left\langle \overline{F}^i \right\rangle \tag{5}$$

Besides these matrices, the scattering of non-deterministic targets can be represented, according to Cloude and Pottier (1996), by power matrices of covariance [C] and coherence [T]. Since the radar image pixels contain many scatterers (especially in the forest targets), with different scattering properties, the covariance and coherence can be used to represent the matrix [S]. The covariance matrix [C] is generated by multiplying the vector-target (Kennaugh) and its joint complex.

$$[C] = \left\langle \vec{K}_c . \vec{K}_c^{*T} \right\rangle \tag{6}$$

where:

$$\vec{k}_c = (S_{hh}, \sqrt{2}S_{hv}, S_{vv})^T ;$$

$$\vec{K}_p = 1/\sqrt{2}\left[(S_{hh} + S_{vv})(S_{hh} - S_{vv})(S_{hv} + S_{vh})i(S_{hv} - S_{vh})\right]^T$$

<…> represents the spatial average.

When one is working with the average value of scattering mechanisms from a pre-defined window in the imaged scene, the characterization of the targets by polarization power is a consequence of a spatial average (normally of pixels), and this operation is called multi-look processing.

On the other hand, the coherence matrix [T], which is related to the physical and geometric properties of the scattering processes, is given by:

$$[T] = \left\langle \vec{K}_p . \vec{K}_p^{*T} \right\rangle \tag{7}$$

Where: $\vec{K}_p$ is the scattering vector written in the Pauli basis (ESA, 2009b)

The matrices [C] and [T] contain the same information about amplitude, phase and correlations, besides its' eigenvalues are real and similar. As a complement, the matrices [M], [K], [C] and [T] are linearly related among them and there are formal methods for transformation among them (Woodhouse, 2006).

The known decompositions to model the nature of coherent targets (represented by the matrix [S]) are those from Pauli, Krogager (SHD), Cameron and Hyunen (Touzi et al., 2004; Zhang et al., 2008), but they are beyond the scope of discussion at this chapter. For non-deterministic targets (represented by second order matrices) there are two decomposition mechanisms implemented at most software packages, which are used for the discrimination of scattering type occurring in forest targets: the decompositions of Freeman-Durden and Cloude-Pottier.

The Freeman-Durden decomposition models the matrix [C] as a contribution of the surface scattering (f_s), the double-bounce (f_d), and volumetric type (f_v) where each type of contribution is represented by the theoretical target, related to the respective type of scattering which occurs at the forest (Freeman and Durden, 1998).

The polarimetric decomposition of Cloude and Pottier (1997) is based on three canonic elements (entropy, anisotropy and alpha angle) defined as a function of the decomposition of eigenvalues and eigenvectors from the matrix [T]:

$$\left\langle \left| T_3 \right| \right\rangle = \sum_{i=1}^{3} \left[T_{3i} \right] = \lambda_1 (e_1 e_1^{*T}) + \lambda_2 (e_2 e_2^{*T}) + \lambda_3 (e_3 e_3^{*T}) \tag{8}$$

Where: λ_i and e_i are eigenvalues and eigenvectors of the matrix [T] respectively.

The entropy *(H)* is a parameter that indicates the type of target involved in the imaged scene and the number of dominant scattering mechanisms (*H~0* = mechanism of unique scattering; *H~1* = multiple scattering mechanisms). In a dense tropical forest, the H values are normally elevated, indicating a larger variation of structural arrangements due to the diversity of species composition, the different levels of competition and growth, as well as the inter-specific association among species. In short, the entropy represents the randomness of the scattering.

The alpha angle (a) indicates the type of scattering dominating the scene, where a = 0° (surface scattering), a = 45° (volumetric scattering) and a = 90° (double-bounce scattering).

The anisotropy (A) is a complementary parameter that measures the relative importance of λ_2 and λ_3 (Equation 8). When $H > 0.7$, the anisotropy contributes with additional information to characterize the target. Below this value, the anisotropy is noisy and has limited

importance. The intensity of these canonic elements identifies the presence of primary or secondary scatterers, and the dominant type of scattering.
The association of entropy (*H*) and alpha angle (*a*) planes is one of the most efficient and usual means of improving the understanding of forest targets. In this classification procedure based on target decomposition, the *H* - *a* components are plotted in a plane with finite zones (Figure 2), which represent scattering mechanisms defined by Cloude and Pottier (1997). These attribute spaces help defining the dominant type of scattering which can be multiple, volumetric or superficial. The theory behind this target decomposition method assumes that the formation of an image is a stochastic process, where an image with a high value of entropy ($0.5 < H < 0.9$) presents much more details.

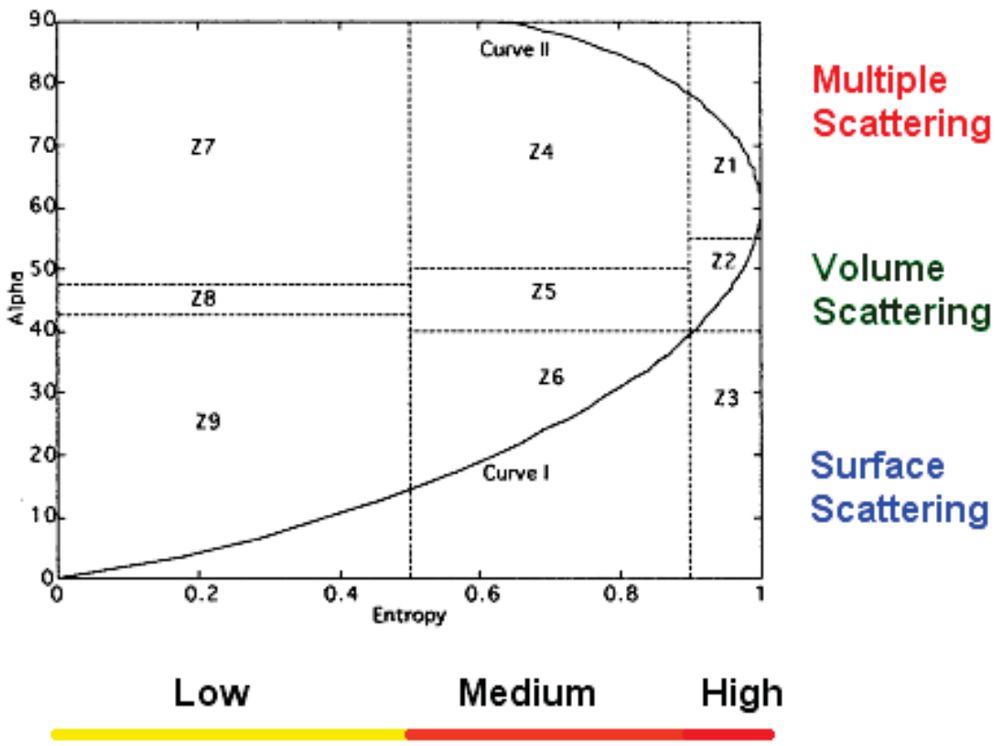

Fig. 2. Schematic diagram of the bi-dimensional classification based on entropy (*H*) and average orientation alpha angle (*a*).
Source: Modified from Cloude and Pottier (1997).

In this procedure of classification by target decomposition, the scattering mechanisms are defined in 9 distinct zones (Figure 2), namely: Z1- High entropy multiple scattering; Z2 - High entropy vegetation scattering; Z3 - High entropy surface scatter; Z4 - Medium entropy multiple scattering; Z5 – Medium entropy vegetation scattering; Z6 – Medium entropy surface scatter; Z7 – Low entropy multiple scattering events; Z-8 – Low entropy dipole scattering; Z9 – Low entropy surface scatter. Within the partition of the plan entropy and angle α in several regions which determine and label the intensity of each scattering

mechanism, it is important to mention that Z3 is outside de representation areas from curves I and II (Figure 2) and so it is not a non-feasible region (Hajnsek et al., 2003), because the polarimetric SAR systems are not able to discriminate high entropy (H > 0.9). The curves I and II represent the borders of values with maximum and minimum observable α angle, as a function of entropy, whose limits are determined by the H- a variation for a coherence matrix with the degenerate minor eigenvalues with amplitude m($0 \leq m \leq 1$), according to the Cloude and Pottier (1997).

1.1.3 Polarization synthesis and signatures

An important aspect for the characterization of forest targets is the polarization synthesis, because when the matrix [S] of a target is known, it is possible to synthesize its backscatter (σ) to any combination of transmitted and received polarization (Ulaby and Elachi, 1990; Woodhouse, 2006). This is a good advantage of polarimetric data, synthesized according to equations 9 and 10:

$$P_{rec}(\psi_r, \chi_r, \psi_t, \chi_t) = \frac{\kappa}{r^2} \cdot \left| \vec{F}^r \cdot [K] \cdot \vec{F}^t \right| \tag{9}$$

$$\sigma_{rt}(\psi_r, \chi_r, \psi_t, \chi_t) = \lim_{r \to \infty} 4\pi r^2 \left(\frac{P_{rt}^{rec}}{P^{trans}} \right) \tag{10}$$

Where: ψ = orientation angle; χ = ellipticity angle; K = vector of target; r = radius.

The polarization states of the electric fields E_v, and E_h which are associated with the radar backscatter (σ) and the dependence of amplitude on polarization, can be represented graphically as a function of ellipticity (χ) and orientation (ψ) angles of the transmitted wave, defining a three-dimensional surface plot called polarization signature or polarization response (Figure 3). The polarization signatures can be used to characterize targets, considering the more detailed knowledge of the mechanisms responsible for the scattering of the radar signal, and the intrinsic target characteristics (van Zyl et al., 1987). It can also be used for the polarimetric calibration of radar data. It is very important to point out that the polarized signature of a certain target is not unique, since different combinations of scattering mechanisms can give a similar configuration, as will be shown in this chapter. This can be due to the structural composition of the forest target, such as the density of trees, regular spatial distribution of trees, trunk diameter and density of twigs and branches, the moisture content in the leaves and in the soil, the dielectric constant of the target under study, etc. In addition, a target can also present distinct polarimetric behavior shown in its signatures, as a function of variations from radar frequency and/or local incidence angle.

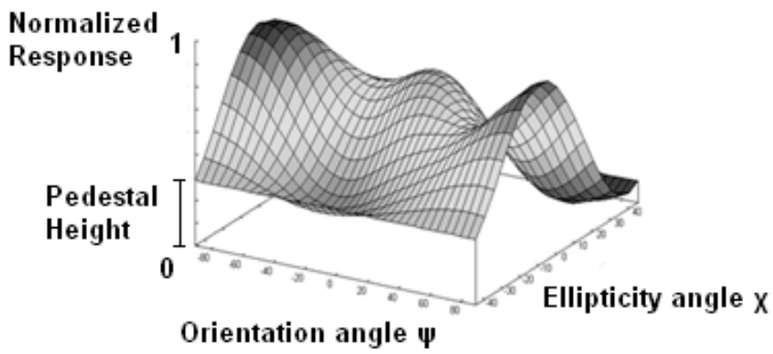

Fig. 3. Polarimetric response of a secondary succession area in the Brazilian Amazon.

It is important to observe in Figure 3 the representation of values of transmitted and received power, where there is a minimum value (pedestal height) of polarization intensity. This minimum value represents the amount of the non-polarized power in the received signal, and thus is related to the polarization level of the scattered wave (CCRS, 2001). If a single target is scattering and the backscattered wave is fully polarized, or if the signature is calculated from a single unaveraged measurement, the pedestal height is zero. But if the signature is calculated from an average of several samples, and there are multiple, dissimilar scatters present or there is noise in the received signal, the pedestal height will be non-zero. Thus the pedestal height is also a measure of the number of different types of scattering mechanism found in the averaged samples. The pedestal of the polarimetric signature may also be a worthy source of information for target characterization (McNairn et al., 2002). In fact, the pedestal corresponds to the ratio of the extreme power received when the antennas are co-polarized or cross-polarized. Therefore, the pedestal provides information equivalent to that obtained with the coefficient of variation by van Zyl et al. (1987). The latter should be more effective because it is not limited to co-polarizations and cross-polarizations (Touzi et al., 2004).

2. ALOS PALSAR data over the Brazilian tropical forest

2.1. Area under study

In order to understand the mechanisms controlling the interaction radar-forest target, a test-site was selected in the Tapajós region (NW Pará State, Brazil), delimited by the geographical coordinates 3º 01′ 60″ - 3º 10′ 39″ S and 54º 52′ 45″ - 54º 59′ 53″ WGr (Figure 4). This region is characterized by a low rolling relief, typical of the lower Amazon plateau and the upper Xingu-Tapajós Plateau. It is dominated by a continuous cover of primary tropical rainforest characterized by the presence on emergent trees and an uniform vegetation cover (Dense Ombrophilous Forests), as well as sections of low to dissected plateaus with few emerging individuals and a high density of palm trees (Open Ombrophilous Forests). The land use is primarily subsistence agriculture, few cash crops, cattle raise and selective logging activities (Figure 5). Areas of secondary succession are also found in different growth stages, resulting from land tracts abandoned after a short period of use, with intensive subsistence agricultural practice or cattle raising.

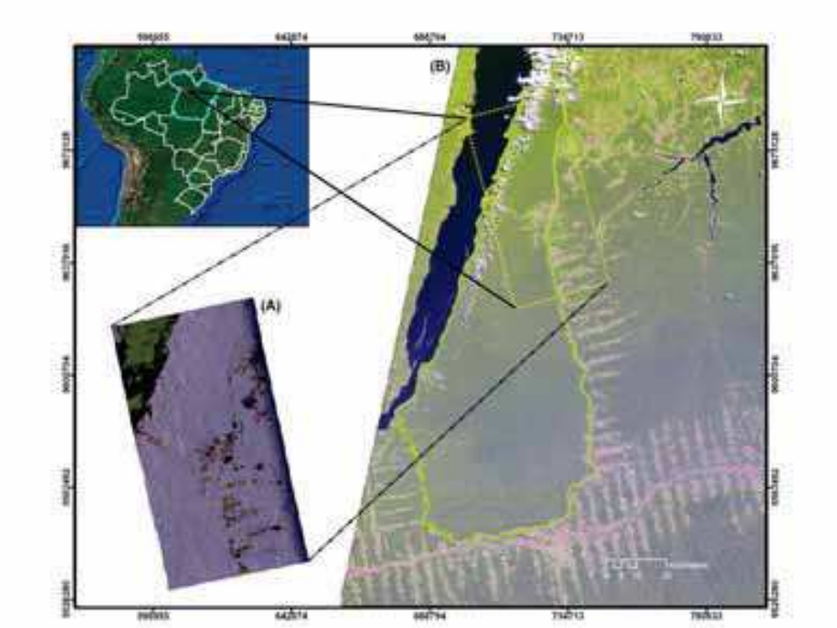

Fig. 4. Study area (dotted rectangle) as shown on LANDSAT/ETM+ (RGB = B3, B4, B5) and ALOS/PALSAR (RGB = HH, HV, VV) images.

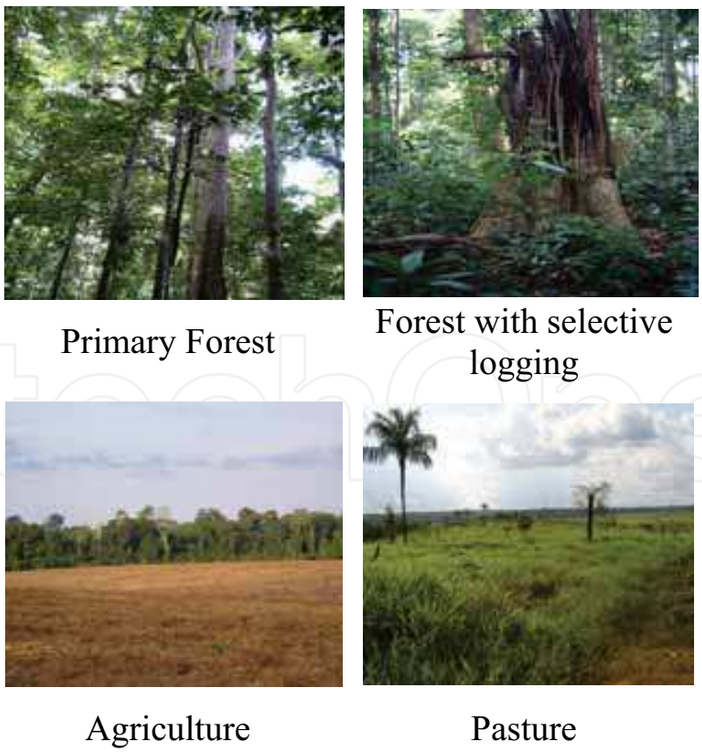

Fig. 5. Land use and land cover classes in the Tapajós region.

2.2 PALSAR image and field data analysis

The *Advanced Land Observing Satellite"* (ALOS) launched on January 24th 2006 has a "Phased-array L-band Synthetic Aperture Radar" (PALSAR) onboard, which was developed by the Japanese Aerospace Exploration Agency (JAXA), with a strategy for multi-temporal imaging, at both regional and global levels. All imaging modes of PALSAR (L- band = 23cm), named as FBS (Fine beam), FBD (Fine beam dual), SCANSAR, DSN (direct transmission) and POL (polarimetric) were calibrated and validated using a total of 500 well-distributed points around the world (Shimada et al., 2007). In this study we used fully polarimetric data (HH, HV, VH and VV polarizations ascending mode), acquired on April 23rd 2007, with a spatial resolution of 4.50m in range and 9.50m in azimuth and an incidence angle of ~ 24º. Using these data studies were done to characterize polarimetric signatures and to gain a detailed understanding of the scattering mechanisms that control the radiation response to the SAR antenna.

2.2.1 Exploratory data analysis

A methodological approach was conducted to explore the sensitivity of two polarimetric techniques in the assessment of structural variations of some land cover classes: primary forest (PF), forest with old timber exploitation (SL) and also, initial (ISS), intermediate (IntSS), and advanced secondary succession (ASS).

The first polarimetric technique involved the generation of graphic representations of the co-polarized SAR response of each forest types, as described by van Zyl et al. (1987). In order to generate the polarization response plots, we used the polarimetric module SPW (PCI (SAR Polarimetry W orkstation) was used (PCI Geomatics, 2007). In this representation, a cross section of a certain type of forest cover (σ) was plotted on a bi-dimensional graphic, as a function of all combinations of orientation angles (ψ) and ellipticity (χ), related to the polarization ellipsis (Ouarzeddine et al., 2007). In order to derive the polarization response for a given region of interest (ROI) - sample area that includes a sufficient number of representative pixels of the theme, reducing the statistical uncertainties and the influence of the speckle noise - at the SAR image, we used the average complex value of all pixels within that ROI. The resulting surfaces were compared by visual inspection, using information on structural characteristics derived from field inventory. It is important to mention that all ROIs represent georeferenced forest inventory plots, where field-based measurements were performed.

In the second exploratory analysis the objective was to performed target decomposition, which expresses the average scattering mechanism of each forest types as the sum of independent elements associated with physical mechanisms. The entropy values and the average alpha angle values of each ROI, (resulting from the decomposition of eigenvalues and eigenvectors of the coherence matrix – see section 1.2.2) were plotted in the bi-dimensional classification space $\left(H,\overline{\alpha}\right)$, following the procedure introduced by Cloude and Pottier (1997).

After including the SAR response of each forest type in the $\left(H,\overline{\alpha}\right)$ bi-dimensional space, the resulting classifications were pair-wise compared using regression analysis technique (Freese, 1964; Neter, 1996). First a linear model was fitted for each classification pair by regressing the percentage number of pixels classified in each zone of the $\left(H,\overline{\alpha}\right)$ plane. The

estimated regression coefficients where then tested to check whether ther fitted line was a 45 degree line through the origin (F test of $b_1 = 0$ versus $b_1 \neq 0$; t test of $b_0 = 0$ versus $b_0 \neq 0$; and t test of $b_1 = 1$ versus $b_1 \neq 1$; where b_0 and b_1 are the regression coefficients). This result would indicate no significant difference between the two tested classifications at the 5% significance level, and therefore no success of the technique in discriminating between the two forest types.

2.2.2 Field survey

In August/September 2007 (same year as the PALSAR data acquisition) a forest inventory was made for the physiognomic-structural characterization of these typologies, to obtain information about the five forest types described above. Tropical forest sections were discriminated by the occurrence (sustainable timber exploitation - SL) or non-occurrence (PF) of human disturbances. In addition, areas of regeneration were studied in order to represent three secondary succession stages, namely: initial (ISS) with age intervals of below 6 years; intermediate (IntSS) from 6 to 15 years; and advanced (ASS) above 15 years. This stratification is considered the age of the natural regrowth as well as structural and floristic characteristics of each seral stage.

Several transects were inventoried to represent each forest typologies. Within these transects, several biophysical parameters were measured, including: diameter at breast height (DBH), commercial and total heights, canopy gap fraction, and location of each arboreal individual in the plot. Additionally, a botanical identification was also performed, according to the field survey procedure described by Santos et al. (2003). As an example to illustrate the importance of accounting for the biophysical parameters collected during the forest inventory to analyze radar data, Figure 6 shows the structural differences between two thematic types, referring to a primary forest and a young natural regrowth.

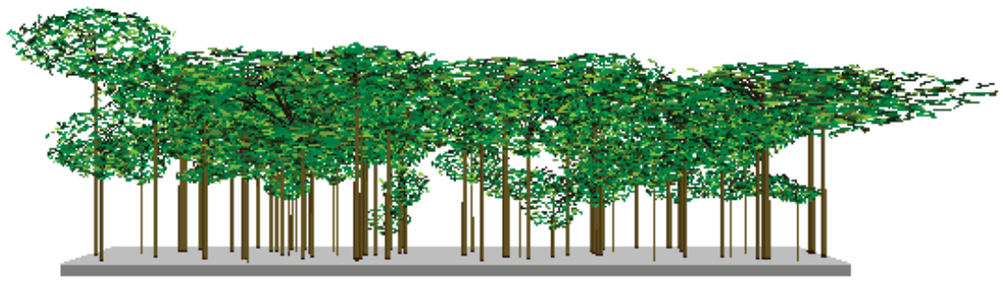

(a)

(b)

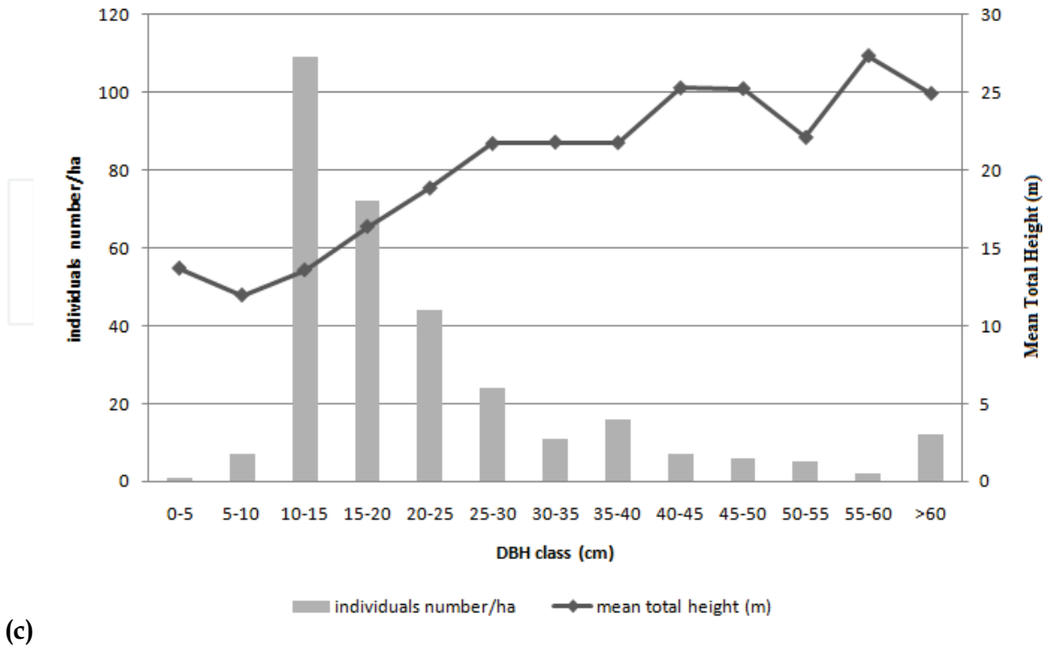

(c)

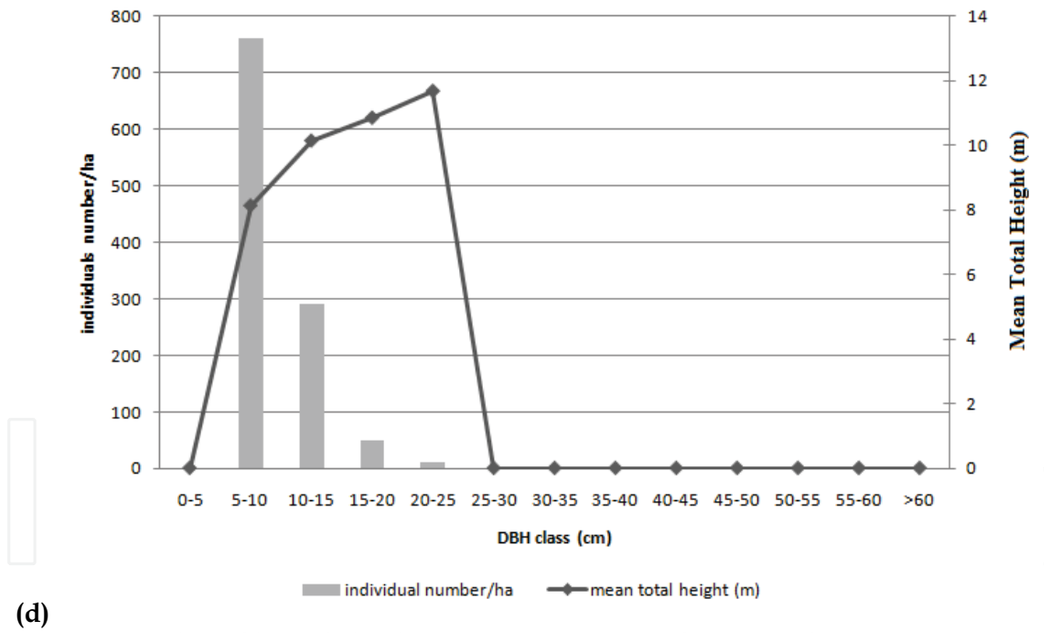

(d)

Fig. 6. Structural profile and dendrometric parameters of primary forest (a, c) and initial secondary succession (b, d), respectively.

2.2.3 Results and discussion

In order to familiarize the reader with the physiognomic-structural features of the forest typology of this section from the Amazon region under study, some results of the field survey are briefly presented.

The initial stage ''capoeiras'' regrowth (ISS) had an average height of 8m and an average DBH of 9cm. Floristic composition was dominated by species such as *Vismia guianensis* (Aubl.) Choisy (Guttiferae), *Cecropia leucoma* Miquel. (Moraceae), *Guatteria poeppigiana* Mart. (Annonaceae), *Aegiphila* sp. (Verbenaceae) and *Cordia bicolor* A. D.C. (Boraginaceae). The intermediate secondary succession (IntSS) had an average height of 11m and an average DBH of 10cm, with a higher abundance of *Cecropia sciadophylla* Mart (Cecropiaceae), *Schizolobium amazonicum* Huber (Fabaceae), *Cassia pentandra* Raddi (Fabaceae), *Vismia japurensis* Reichardt and *Vismia guianensis* (Aubl.) Choisy. (Guttiferae). The advanced secondary succession (ASS) had an average height of 18m and average DBH of 25cm with species *Bagassa guianensis* Aubl. (Moraceae), *Guatteria poeppigiana* Mart. (Annonaceae), *Casearia decandra* Jacq. (Flacourtiaceae), *Cassia pentandra* Raddi (Fabaceae), *Couratari oblongifolia* Ducke & R. Knuth (Lecythidaceae), and *Apeiba albiflora* Ducke (Malvaceae).

The primary forest stands (PF) present 3 to 4 strata with about 360 trees per hectare, whose upper stratum shows individuals with an average height of 21 m and DBH of 27 cm. The botanical diversity of the primary forest was significantly higher compared to areas of secondary succession, being dominated by species such as: *Protium apiculatum* Swart (Burseraceae), *Picrolemma sprucei* Hook (Simaroubaceae), *Rinorea guianensis* (Aubl.) Kuntze (Violaceae), *Cordia bicolor* A.DC. in DC. (Boraginaceae), *Jacaranda copaia* D.Don (Bignoniaceae), *Pouteria* sp. (Sapotaceae) and *Inga* sp. (Fabaceae). The primary forest stands that were affected by timber exploitation (SL) present a decrease of timber volume of around 27.3 m^3/hectare, which corresponds to an average density of exploration of 3.3 trees/ha, in accordance with the forest management plan formerly established by IBAMA/PNUD (1997). At the gaps resulting from the extraction of trees with commercial value and also at the trails where tree trunks were dragged, quickly pioneer species install themselves, such as *Cecropia leucoma* Miquel, *Cecropia sciadopylla* Mart., and *Guatteria poeppigiana* Mart., modifying the environment and providing resources for other species.

The description above suggest that there is a distinct frequency of trees by diameter and height class, as well as the occurrence of characteristic species in each forest types, which model the physical space under study. There is a positive gradient in these two ecological parameters, increasing from initial secondary succession until a mature forest. One observes that at the initial regrowth there is a more uniform canopy formed by 1 or 2 strata of low height, with pioneer species with thinner trunks found repeatedly in the area, from a few botanical families (Figure 6). The older secondary succession stages, the higher is the structural complexity, characterized by a wide variation in tree size, with a stepwise replacement of pioneer species and the formation of multiple canopy layers. A detailed description of the floristic composition and structure of forest typology from the Tapajós region can be found at Gonçalves (2007) Gonçalves and Santos (2008). The considerations above are important to facilitate the understanding of the polarized response.

At Figure 7 the shape features of co-polarization signatures derived from the PALSAR data of the 11 ROIs are presented, which were selected to represent the diversity of the tropical forest in Tapajós region. In all the polarization signature plots presented, the maximum intensity has been normalized to 1.0, according to Ouarzeddine et al. (2007). Before discussing this subject it is important to remind that in theory, in the co-polarization response, taking into account the representation in a plane ($-90^o < \psi < +90^o$), the highest values of intensity for an ellipticity angle at 0^o and an orientation angle at 0^o, the polarization is horizontally oriented (Evans et al., 1988; Mc Nairn et al. 2002).

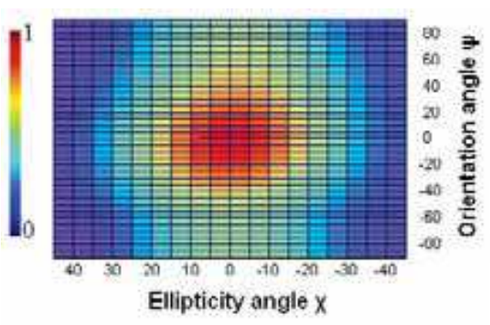

P1

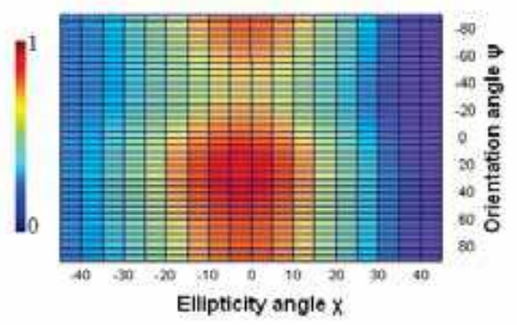

P2

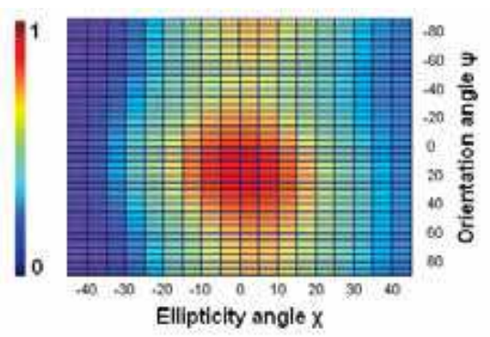

P3

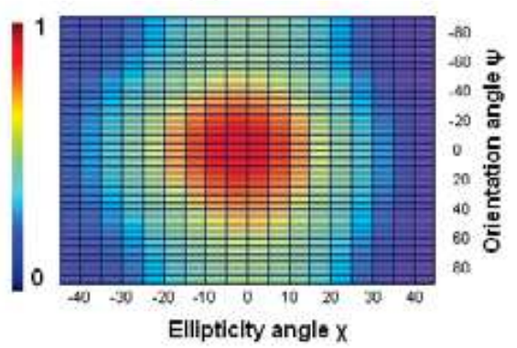

P4

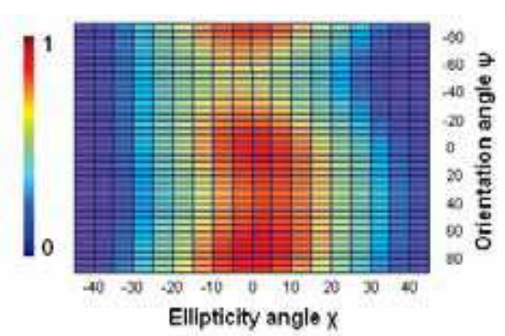

P5

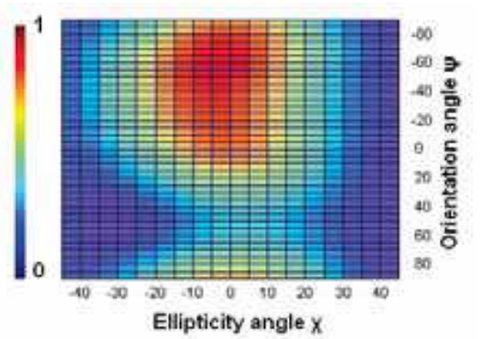

P6

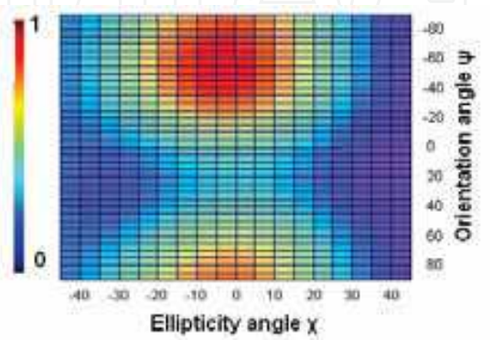

P7

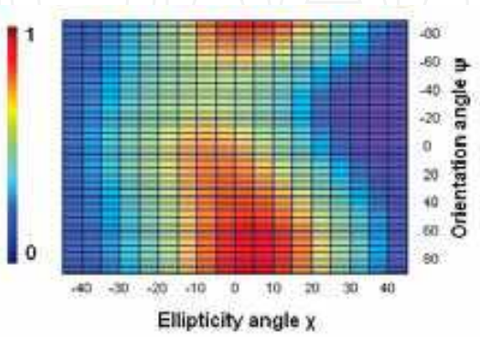

P8

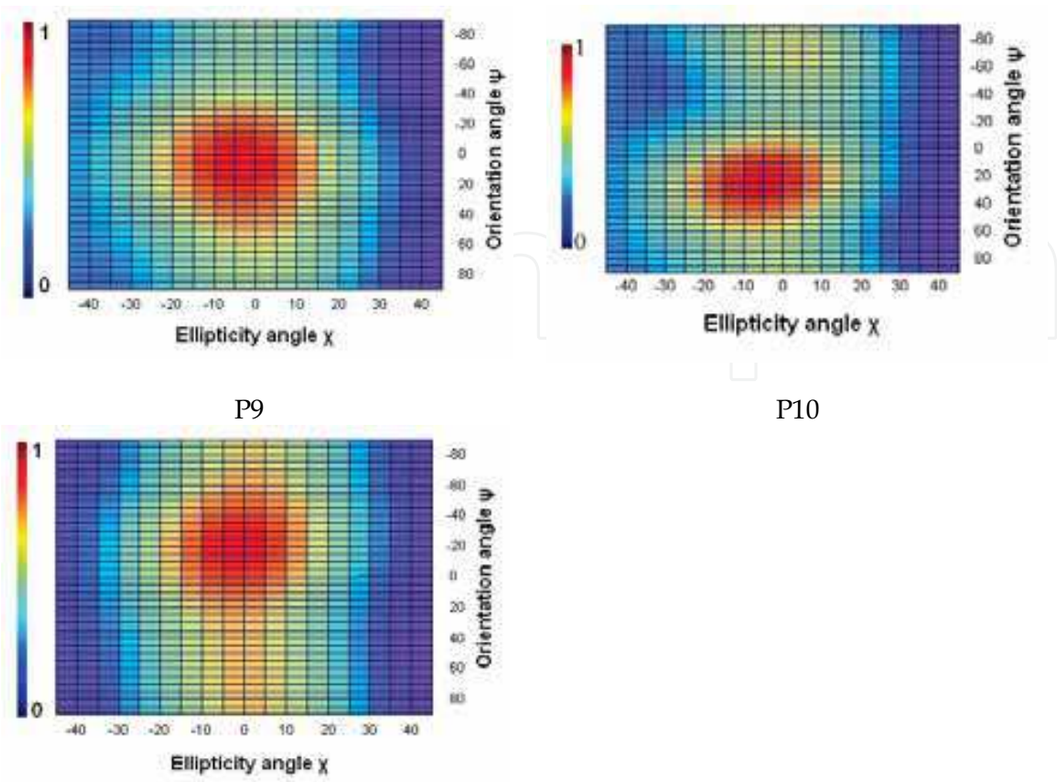

Fig. 7. Polarization responses derived from at PALSAR data acquired in the Tapajós region, Brazil. Targets include primary forest (P1, P2), forest with old selective logging (P3, P4, P5), advanced secondary succession (P6, P7), intermediate secondary succession (P8, P9) and initial secondary succession (P10, P11).

The polarization responses of samples of ASS (P6, P7), IntSS (P8) and ISS (P10, P11) show a strong similarity to the theoretical responses of short and thin conducting cylinders (i.e. radius and lengths much shorter than the wavelength). This suggests that the scattering produced by twigs and small branches has an important contribution for the total backscattering of these regrowth types. The co-polarized response of samples P6 and P7 (both old regrowth) with ψ = - 70º and P8 (intermediate regrowth) with ψ = ± 90°, show stronger returns at VV than HH, consistent with increased double reflections and present diffusers with preferentially vertical orientation. The responses of the other analyzed areas (i.e. P10, P11) indicate the predominance of branches oriented at ±45º in relation to the horizontal plane, possibly due to more homogeneous canopies of these younger recovery sections with low species diversity and a quite uniform growth rate (height intervals of 6 to 9 m corresponds to 90% of the trees) (Figure 6). One must emphasize that, taking into account the distinction of the stands investigated, the polarization responses of sections P7 and P10 are similar to those presented by Ulaby and Elachi (1990), but with maximum co-polarized power at ψ = - 60º and χ = 0º for P7 sample and maximum co-polarized response at ψ = 30º and χ = -5º for P10 site and with a thin cylinder oriented vertically.

The polarization signatures of plots P1 and P2 (primary forest), P4 and P5 (forest under exploitation) and also P9 (intermediate secondary succession), are similar those of trihedral corner reflectors, which have a double bounce scattering geometry, when one of the reflector sides is parallel to the line connecting the radar antenna and the corner reflector, as mentioned by Zebker and Norikane (1987). For sections of more complex forest structures, the highest σ values occur in linear polarizations, with a certain independence of the orientation angle (ψ). This can be observed in plots P1, P2, P3 and P4, which represent the mature forest (with or without legal selective logging), whose concentrated section of maximum co-polarized power occurs in a range of $\psi = 0°$ to $\pm 20^o$ when $\chi = 0^o$. As for forest areas affected by timber exploitation, one expects predominance of double-bounce scattering, due of the larger number of gaps resulting from the removal some trees with commercial value and also because this type of mature forest has a well-defined vertical structure in various strata with a much thinner undergrowth. Specifically, for the plot P3 presents most diffusers oriented horizontally ($\psi = 0$) and it has a stronger return at HH than VV, where the maximum for this signature seems slightly shifted from the horizontal position towards the vertical. This effect might be explained by the presence of the topographic slopes in the azimuth direction. In additional, medium or high impact logging practices can increase the structural heterogeneity, causing changes in the polarization response of the forest target investigated.

At the analysis of polarimetric signatures, the height of the pedestals must also be considered because it provides an additional source of information for target characterization, and to provide information similar to that obtained with the variation coefficient (van Zyl et al, 1987; Mc Nairn et al, 2002). Contrary to expected, in the co-polarized response derived from PALSAR, the highest pedestals occur for areas of secondary succession if compared to those of forest typologies, suggesting the existence of a considerable variation on the scattering properties of the adjacent resolution elements. The highest values of 0.313 and 0.333 were found respectively for areas of initial (P10) and intermediate (P8) recovery, respectively. Old-growth forests, with or without timber exploitation (P1, P2, P3 and P4) showed pedestal height ranging from 0.068 to 0.195. Within the characteristics of natural forest stands, the lower branch density can explain the lower values of pedestal height, which results at a lower non-polarized power component in the backscatter, indicating a smaller amount of volume scattering (CCRS, 2001). Note that, in contrast to our findings, previous studies conduced in tropical zones using SAR data have shown that a higher age and diversity of species and consequently, a stronger variability of forest structure, results at an increase of the pedestal size on the polarization responses.

In tropical areas with complex vegetation types, the polarimetric signature of each type is really not unique. One can simply observe that areas of early secondary succession could, for instance, could have its' growth influenced by aspects, such as: previous land use, soil fertility level, bio-ecological level of fragmentation, etc. From measurements performed during field survey we also verified that the canopy was more open in sites of initial regrowth, localized over areas with low soil fertility and a history of more intensive use, compared to those with higher soil fertility and a less intensive land use, both areas with the same age of natural succession. During the intermediate phase of secondary succession, the canopy remains more open, and the mortality of some pioneer species which are not tolerant to shadow is higher, but presenting a larger vertical stratification. With the increase of age from the natural regrowth, the horizontal and vertical structures become more

complex, presenting biophysical characteristics close to those of primary forest. Such biophysical arrangements, which include the structure/density of the canopy, the occurrence of a larger or smaller number of arboreal/bush individuals (scatterers) in these types of vegetation formations, can lead to distinct polarimetric intra-class and inter-class configurations, with pedestal height values which are also different, as observed on Figure 7. Figure 8 shows the distribution of pixels extracted from the eleven ROIs in the bi-dimensional classification space $(H, \overline{\alpha})$, whose numerical results (i.e., percent of pixels by scattering zone) are presented in Table 1. At Figure 8 one observes that all 7 ROIs representative of primary forest, forest with timber exploitation and advanced secondary succession, show a concentrated pixel distribution (~70%) at zones Z4, Z5 and Z9. This indicates that the polarimetric response of such classes from already defined forest structure (containing 3 or 4 strata) is based mainly on multiple and volumetric scattering (the backscattering signal is mainly a function of geometry of scatters elements from dense cover) at zones of medium entropy. Additionally there is also some influence of a surface scattering but derived from a zone of low entropy. The two representative plots of classes from intermediate recovery have a higher distribution of pixels (>60%) at the zone of medium entropy (Z5), due to dipole scattering objects and in zones of low entropy (Z9, Z7), with scattering objects regularly distributed in space, and also as a consequence of the double-bounce effect caused by scattering objects such as twigs-trunk-soil-trunk. The initial secondary succession is positioned preferentially in the space of attributes of low entropy (Z9) and also configured by double-bounce interaction mechanisms (medium entropy multiple scattering – Z4), affected by the propagation of the canopy, as a result of the growth uniformity of pioneer species where there is a predominance of only an upper homogeneous stratum, and a lower dispersed one, formed by small plants which germinate and develop in a late succession process, in the shadow of the pioneers.

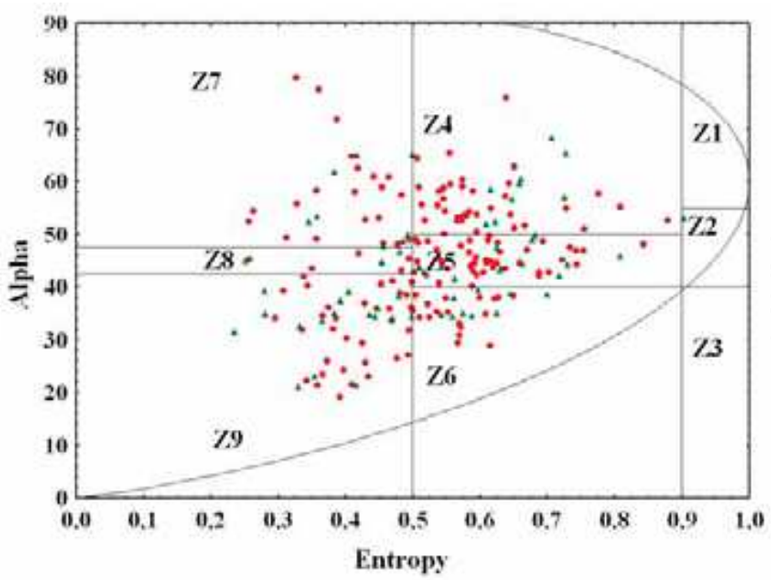

Fig. 8. L-band PALSAR α-*H* distribution for scattering mechanism: green colour are pixels of primary forest, forest with old selective logging and advanced secondary succession; red colour are initial and intermediate secondary succession. Source: Santos et al. (2009).

Zones	ROIs (Vegetation Types)										
	PF			SL		ASS		IntSS		ISS	
	P1	P2	P3	P4	P5	P6	P7	P8	P9	P10	P11
Z1	0	0	0	0	0	0	0	0	0	0	0
Z2	0	0	0	0	0	0	0	0	0	0	3.7
Z3	0	0	0	0	0	0	0	0	0	0	0
Z4	8.16	20.4	14.89	35.29	24.49	24.24	42.86	18.52	0	10	33.33
Z5	46.94	26.5	29.79	21.57	14.29	30.3	17.86	14.81	50	26.67	3.7
Z6	8.16	10.2	10.64	11.76	10.2	18.18	3.57	11.11	11.54	13.33	14.81
Z7	10.2	18.4	10.64	17.65	18.37	15.15	7.14	7.41	11.54	13.33	18.52
Z8	12.24	4.1	0	3.92	2.04	0	0	7.41	7.69	6.67	0
Z9	14.29	20.4	34.04	9.8	30.61	12.12	28.57	40.74	19.23	30	25.93

Table 1. Percentual of pixels distribution of each ROI at zones of two-dimensional classification space $(H, \overline{\alpha})$.

The statistical tests used to detect variations among classifications of pairs of ROIs, at 5% significance values, indicate that there present no significant differences. Low p values were observed when comparing SL/ASS, PF/ASS and SL/IntSS, with values of 0.1725, 0.2661 and 0.2754 respectively, which correspond to the largest differences found in polarimetric responses among pairs of ROIs, but they are not significant. Since there are physiognomic-structural differences in forested targets (with or without timber exploitation) and those at younger secondary successional stages, one can infer that, at this level of significance (5%), this classification procedure $(H, \overline{\alpha})$ by target decomposition of the PALSAR data was not enough robust to detect such a variability. As observed during the previous discussion, we made the identification and definition of intensity for each scattering mechanism of the pixels contained in the PALSAR image, corresponding to each type forest typology, within these zones of the alpha-entropy space. This procedure should facilitate the attribution of each zone to a certain thematic class. But, due to the structural complexity and floristic diversity of the tropical landscape investigated and of its intrinsic scatterers, in this case there was a limitation to the procedure described by Cloude and Pottier (1997), because there is a fixed position of the decision borders of the classifier used. Nevertheless, from this partition of the alpha-entropy plan, new approaches which consider statistical modelling to treat POLSAR data (Pottier and Lee, 2000; Ferro-Famil et al., 2008) are being used with a relative success, as shown by Freitas et al. (2008), for the analysis of land use/land cover of a section from the Amazon region.

3. Conclusions

This chapter gave an overview of the utility from SAR polarimetric data to discriminate tropical forest types, whose analysis procedures were based on the knowledge of the shape from the co-polarized signature and also on the type and intensity of the dominant scattering mechanisms. All this allows the analyst to distinguish the space of attributes occupied by features of a tropical landscape and to establish which parameters are more efficient for a thematic discrimination. It allows also to define the level of agglutination among typologies, of subtle physiognomic-structural gradients at a classification from SAR images.

Taking into account the experience gathered with the use of ALOS/PALSAR data (L-band) in the Brazilian Amazon, based on the classification by target decomposition supported by information derived from forest inventories, the following conclusions are made: (a) at several types of landscapes studied there is a predominance of scattering processes with medium entropy, with volumetric and multiple scattering, influencing mainly those structures with more forests; (b) areas under natural recovery (initial or intermediate) present mechanisms of surface type (low entropy) and double-bounce affected by canopy propagation (medium entropy); (c) the classification method by target decomposition based on entropy values and of the mean alpha angle was not robust enough to detect the floristic-structural variability existing among certain land cover classes; (d) the parallel polarization responses obtained from several forest cover classes show different configurations, indicating that the backscatter of certain plots was dominated by distinct physical mechanisms. A more detailed analysis of species composition and its arrangements and proportions as dominant and co-dominant in the vertical structure of forest stands must be done, in order to improve understanding of different co-polarized signatures and the interaction mechanisms that command the radar signal and the target. The analysis of PALSAR cross-polarized mode data is another approach under development. Presently, we are analyzing cross-polarized PALSAR data aiming at a higher accuracy at the thematic classification as a consequence we are expecting an improvement of biomass modelling in tropical forest.

4. Acknowledgements

We acknowledge to CNPq for the research grants; the IBAMA/MMA and LBA for the logistic support in the study. We also thank our colleagues J. C. Mura, F. F. Gama, A. S. Queiroz, S. J. S. Sant'Anna, H. J. H. Kux (INPE) and Jakob van Zyl (JPL/NASA) for discussions during the development of this chapter.

5. References

Andersen, L.; Granger, C.; Reis, E.; Weinhold, D.; Wunder, S. (2002). The dynamics of deforestation and economic growth in the Brazilian Amazon. Cambridge: Cambridge University Press. 259p. [ISBN 0 521 81197 X].

Beaudoin, A.; Le Toan, T.; Goze, S.; Nezri, E.; Lopez, A.; Mougin, E.; Hsu, C.C.; Han, H.C.; Kong, J.; Shin, R.T. (1994). Retrieval of forest biomass from SAR data. International Journal of Remote Sensing, 15(14): 2777-2796.

Canada Centre of Remote Sensing - CCRS, (2001). Radar polarimetry: advanced radar polarimetry tutorial. In: Fundamentals of Remote Sensing. 97p. <http://ccrs.nrcan.gc.ca/resource/tutor/polarim/pdf/polarim_e.pdf>.

Cloude, S. R.; Pottier, E. (1997). An entropy based classification scheme for land application of polarimetric SAR. IEEE Transactions on Geoscience and Remote Sensing, 35(1): 68-78.

Cloude, S.R.; Pottier, E. (1996). A review of target decomposition theorems in radar polarimetry. IEEE Transactions on Geoscience and Remote Sensing, 34 (2): 498-518.

Coops, N.C. (2002). Eucalyptus forest structure and synthetic aperture radar backscatter: a theoretical analysis. Trees, 16: 28-46.

Cressie, N. A. (1993). Statistics for spatial data, New York: John Wiley & Sons. 900p.

European Space Agency – ESA. (2009a). Single vs multi polarization SAR data. 28p. <http://earth.esa.int/polsarpro/tutorial.html>.

European Space Agency – ESA. (2009b). Polarimetric decompositions. 28p. <http://earth.esa.int/polsarpro/tutorial.html>.

Evans, D. L.; Farr, T. G.; van Zyl, J. J; Zebker, H. A. (1988). Radar polarimetry: analysis tools and applications. IEEE Transactions on Geoscience and Remote Sensing, 26(6): 774 – 789.

Ferro-Famil, L.; Pottier, E.; Lee, J. S. (2001). Unsupervised classification of multifrequency and fully polarimetric SAR images based on the H/A/Alpha-Wishart classifier. IEEE Transactions on Geoscience and Remote Sensing, 39(11): 2332-2342.

Freeman, A.; Durden, S. L. A. (1998). Three-component scattering model for polarimetric SAR data. IEEE Transactions on Geoscience and Remote Sensing, 36(3): 963-973.

Freese, F. (1964). Linear regression methods for forest research. U.S. Forest Services Research, Madison, Wisconsin.138p.

Freitas, C. C.; Soler, L. S.; Sant'Anna, S., J. S.; Dutra, L. V.; Santos, J. R.; Mura, J. C.; Correia, A. H. (2008). Land use and land cover mapping in the Brazilian Amazon using polarimetric airborne P-band SAR data. IEEE Transactions on Geoscience and Remote Sensing, 46(10): 2956 – 2970.

Gonçalves, F. G. (2007). *Avaliação de dados SAR polarimétricos para estimativa volumétrica de florestas tropicais*. São José dos Campos, Brazil, Master in Degree in Remote Sensing at National Institute for Space Research. INPE:14777-TDI/1230. 107p.

Gonçalves, F. G.; Santos, J. R. (2008). Composição florística e estrutura de uma unidade de manejo florestal sustentável na Floresta Nacional do Tapajós, Pará. Acta Amazonica, 38(2): 229-244.

Hajnsek, I.; Pottier, E.; Cloude, S. R. (2003). Inversion of surface parameters from polarimetric SAR. IEEE Transactions on Geoscience and Remote Sensing, 41(4): 727-739.

Hawkins, R. K.; Attema, E.; Crapolicchio, R.; Lecomte, P.; Closa, J.; Meadows, P. J.; Srivastava, S. K. (2000). Stability of Amazon backscatter at C-band: spaceborne results from ERS-1/2 and Radarsat-1. In: SAR Workshop – CEOS Committee on Earth Observation Satellites. Toulouse, France, 26-29 Oct., 1999. Edited by Robert A. Harris and L. Ouwenhand. Publisher: Paris, European Space Agency, ESA-SP, vol.450, p.99-108. (ISBN:9290926414).

Hendersen, F. M.; Lewis, A. J. (1998). Radar fundamentals: The geoscience perspective. In: Ryerson, R.A. ed., Principles & Applications of Imaging Radar. Manual of Remote Sensing, 3. ed. New York, John Wiley & Sons, Inc., vol.2, cap.3, p.131-181.

Hoekman, D. H.; Quinones, M. J. (2000). Land cover type and biomass classification using AirSAR data for evaluation of monitoring scenarios in the Colombian Amazon, IEEE Transactions Geoscience and Remote Sensing, 38 (2):.685–696.

Instituto Brasileiro do Meio Ambiente e dos Recursos Naturais Renováveis/Programa das Nações Unidas para o Desenvolvimento - IBAMA/PNUD. (1997). Plano de manejo florestal da Floresta Nacional do Tapajós, Pará, Brasil. IBAMA, Brasília, Distrito Federal. 109pp.

Kugler, F.; Papathanassiou, K. P.; Hajnsek, I. (2006). Forest height estimation over tropical forest by means of polarimetric SAR interferometry. In: Seminário de Atualização em Sensoriamento Remoto e Sistemas de Informações Geográficas Aplicados à Engenharia Florestal, 7., Curitiba, Paraná, 17-19 out., 2006. Anais. pp.504-512. [CDROM].

McNairn, H.; Duguay, C.; Brisco, B.; Pultz, T.Z. (2002). The effect of soil and crop residue characteristics on polarimetric radar response. Remote Sensing of Environment, 80(2): 308-320.

Neeff, T.; Biging, G. S.; Dutra, L. V.; Freitas, C. C.; Santos, J. R. (2005b). Markov point processes for modeling of spatial forest patterns in Amazonia derived from interferometric height. Remote Sensing of Environment, 97: 484 – 494.

Neeff, T. ; Dutra, L. V. ; Santos, J. R.; Freitas, C. C.; Araujo, L. S. (2005a). Power spectrum analysis of SAR data for spatial forest characterization in Amazonia. International Journal of Remote Sensing, 26(13): 2851-2865.

Neter, J.; Kutner, M. H.; Nachtsheim, C. J.; Wasserman, W. (1996). Applied linear statistical models. 4.ed. Boston: McGraw-Hill. 1408 p.

Ouarzeddine, M.; Souissi B.; Belhadj_Aissa, A. (2007). Classification of polarimetric SAR images based on scattering mechanisms. In: Spatial Data Quality, 12-15 June, 2007. ITC, Enschede. http://www.itc.nl/ISSDQ2007/proceedings/poster.html

PCI Geomatics. (2007). Geomatica SPW 10.1 User Guide (SAR Polarimetry Workstation), PCI Geomatics Enterprises Inc., Richmond Hill Ontario, Canada, 179 pp.

Pope, K. O.; Rey-Benayas, J. M.; Paris, J. F. (1994). Radar remote sensing of forest and wetland ecosystems in the Central American tropics. Remote Sensing of Environment, 48(2): 205-219.

Pottier, E.; Lee, J. S. (2000). Unsupervised classification scheme of POLSAR images based on the complex Wishart distribution asnd the H/A/Alpha – Polarimetric decomposition theorem. In: European Conference on Synthetic Aperture Radar, 3, 2000, Munich, Germany. Proceedings. [CDROM].

Santos, J. R.; Freitas, C. C.; Araujo, L. S.; Dutra, L. V.; Mura, J. C.; Gama, F. F.; Soler, L. S.; Sant'Anna, S. J .S. (2003). Airborne P-band SAR applied to the aboveground biomass studies in the Brazilian tropical rainforest. Remote Sensing of Environment, 87(4): 482-493.

Santos, J. R., Mura, J. C., Paradella, W. R., Dutra, L. V. ; Gonçalves, F. G. (2008). Mapping recent deforestation in the Brazilian Amazon using simulated L-band MAPSAR images. International Journal of Remote Sensing, 29(16): 4879 - 4884.

Santos, J. R.; Narvaes, I. S.; Graça, P. M. L. A.; Gonçalves, F.G. (2009). ALOS PI 2008 Symposium. Proceedings, Nov., 3-7th, 2008., Island of Rhodes, Greece. (ESA-664).

Santos, J. R.; Pardi Lacruz, M. S.; Araujo, L. S.; Keil, M. (2002). Savanna and tropical rainforest biomass estimation and spatialization using JERS-1 data. International Journal of Remote Sensing, 23(7):1217-1229.

Shimada, M.; Isoguchi, O; Tadono, T., Higuchi, R.; Isono, K. (2007). PALSAR CALVAL – Summary and update 2007. IEEE Transactions on Geoscience and Remote Sensing, p. 3593-3596.

Touzi, R.; Boerner, W. M.; Lee, J. S.; Lueneburg, E. (2004). A review of polarimetric in the context of synthetic aperture radar: concepts and information extraction. Canadian Journal of Remote Sensing. 30 (3): 380-407.

Treuhaft, R. N.; Chapman, B.; Dutra, L.V.; Gonçalves, F. G.; Santos, J. R.; Mura, J. C.; Graça, P. M. L. A.; Drake, J. (2006). Estimating 3-dimensional structure of tropical forest from radar interferometry. Ambiência, 2(1): 111-119.

Ulaby, F. T.; Elachi, C. (1990). Radar polarimetry for geoscience applications. Norwood: Artech House, Inc., 388 p.

van der Sanden, J. J. (1997). Radar remote sensing to support tropical forest management. Tropenbos-Guyana Series 5: Georgetown, Guyana, PhD Thesis Wageningen Agricultural University. ISBN: 90-5485-778-1. 330p.

van Zyl, J. J., Zebker H. A., Elachi C. (1987). Imaging radar polarimetric signatures: theory and observation. Radio Science, 22(4): 529-543.

Woodhouse, I. H. (2006). Introduction to microwave remote sensing. Boca Raton: CRC Press Taylor & Francis Group, 370p.

Wulder, M.; Niemann, K.; Goodenough, D. (2000). Local maximum filtering for the extraction of tree locations and basal area from high spatial resolution imagery. Remote Sensing of the Environment, 73(1): 103-114.

Zebker, H. A.; Norikane, L. (1987). Radar polarimeter measures orientation of calibration corner reflectors. In: Proceedings of the IEEE, vol. 75, n° 12, pp. 1686-1688.

Zhang, L.; Zhang, J.; Zou, B.; Zhang, Y. (2008). Comparison of methods for target detection and applications using polarimetric SAR image. PIERS Online, 4(1): 140-145.

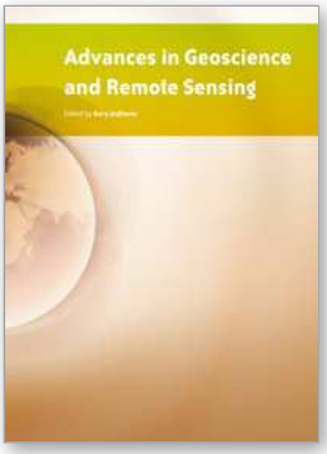

Advances in Geoscience and Remote Sensing

Edited by Gary Jedlovec

ISBN 978-953-307-005-6

Hard cover, 742 pages

Publisher InTech

Published online 01, October, 2009

Published in print edition October, 2009

Remote sensing is the acquisition of information of an object or phenomenon, by the use of either recording or real-time sensing device(s), that is not in physical or intimate contact with the object (such as by way of aircraft, spacecraft, satellite, buoy, or ship). In practice, remote sensing is the stand-off collection through the use of a variety of devices for gathering information on a given object or area. Human existence is dependent on our ability to understand, utilize, manage and maintain the environment we live in - Geoscience is the science that seeks to achieve these goals. This book is a collection of contributions from world-class scientists, engineers and educators engaged in the fields of geoscience and remote sensing.

InTech Europe
University Campus STeP Ri
Slavka Krautzeka 83/A
51000 Rijeka, Croatia
Phone: +385 (51) 770 447
Fax: +385 (51) 686 166
www.intechopen.com

InTech China
Unit 405, Office Block, Hotel Equatorial Shanghai
No.65, Yan An Road (West), Shanghai, 200040, China
中国上海市延安西路65号上海国际贵都大饭店办公楼405单元
Phone: +86-21-62489820
Fax: +86-21-62489821

IntechOpen